49th AIAA Aerospace Sciences Meeting including the New Horizons Forum and Aerospace Exposition
4 - 7 January 2011, Orlando, Florida
AIAA 2011-912

# Jet Noise Shielding for Advanced Hybrid Wing-Body Configurations

Dimitri Papamoschou* and Salvador Mayoral†
*University of California, Irvine, CA 92697, USA*

**We present an experimental study of jet noise shielding with an advanced design for the Hybrid Wing-Body airplane. The design, called N2AEXTE, features an extended trailing edge over its predecessor, the N2A. Static acoustic tests were conducted at a scale factor of 90 with realistic exhaust conditions of a bypass ratio 10 nozzle. The acoustic data show cumulative (downward +sideline) EPNL reductions of up to 10 dB with the nozzle at its nominal position and up to 13 dB with the nozzle traversed upstream by one fan diameter. These reductions are 2-3 dB better than with the basic N2A design. Redistribution of the jet noise source and incorporation of inboard vertical fins are essential elements for achieving those reductions. Devices used to alter the jet noise source comprised aggressive chevrons, a porous wedge fan flow deflector, and their combination. Two shapes for the vertical fins were tested - a nominal design and an alternate design featuring longer chord and shorter height. The alternate fin design offered slight noise benefits.**

## Nomenclature

| | | |
|---|---|---|
| $D$ | = | nozzle exit diameter |
| $f$ | = | frequency |
| $M$ | = | Mach number |
| $R$ | = | distance from nozzle plug tip to microphone |
| $Sr$ | = | Strouhal number = $fD_s/U_s$ |
| $u$ | = | mean axial velocity in the jet plume |
| $U$ | = | nozzle exit velocity |
| $x, y, z$ | = | axial, transverse, and spanwise coordinates relative to plug tip |
| $X$ | = | axial distance between fan exit plane and shield trailing edge |

*Subscripts*

| | | |
|---|---|---|
| $p$ | = | primary (core) exhaust |
| $s$ | = | secondary (fan) exhaust |

## I. Introduction

This study is motivated by the development of ultra-quiet advanced aircraft that will meet NASA's N+2 and eventually N+3 noise goals of 42 and 71 dB, respectively, relative to the Stage 4 baseline. Whether the aircraft are powered by turbofan or open-rotor engines, the noise reduction goals are unlikely to be met without exploiting the propulsion-airframe integration that will reduce the noise emitted towards the community. The advent of the Hybrid Wing-Body (HWB) airplane[1], with the engines mounted over the wing, has reinvigorated the engine over-the-wing (OTW) concept for noise shielding, an area of active research in the 1970s[2-4]. The HWB design allows sufficient planform area for shielding of both the forward-emitting turbomachinery sources and the aft-emitting jet noise sources.

The research team at U.C. Irvine has engaged in experimental[5,6] and computational[7] studies to predict the potential of jet noise shielding for canonical and HWB-type configurations. In our subscale facility we demonstrated significant potential for jet noise shielding using the "N2A" initial design of the HWB, with cumulative EPNL reductions of up to 7.5 dB[6]. An important finding was that jet noise shielding was marginal unless the noise source was altered using devices such as chevrons or fan flow deflectors. Large-scale tests at Boeing, using similar shield and nozzle arrangements, confirmed those noise reduction trends and included the element of forward flight[8]. However, the N2A configuration has inherent aerodynamic challenges when placing the

* Professor, Department of Mechanical and Aerospace Engineering, dpapamos@uci.edu, Fellow AIAA.
† Graduate Student Researcher, Department of Mechanical and Aerospace Engineering, smayoral@uci.edu. AIAA Student Member.

engines sufficiently upstream to obtain satisfactory jet noise shielding. Consequently, Boeing designed an advanced, extended-trailing-edge version of the N2A, called N2AEXTE. The extended trailing edge enables sufficient surface area between the nozzle exit and the trailing edge without exposing the engines to high-transonic Mach numbers that can seriously penalize its aerodynamic performance. The present work is a follow-up to our past study, using the N2AEXTE as the shielding planform. We investigate source compaction/redistribution devices in association with varying designs for the vertical fins and axial placement of the nozzle.

## II. Experimental Details

### A. Nozzle and Shield Configurations

Subscale jet noise shielding experiments were carried out with a nozzle–shield configuration composed of a dual-stream nozzle with an N2AEXTE-shaped shield, as depicted in Fig. 1. The scale factor was 90. The HWB shield has two types of vertical fins, shown in Fig.2. The baseline nozzle is designed for a bypass ratio 10 and has a secondary (fan) diameter $D_s$ =31.2 mm and fan exit height of 4.0 mm. The nozzle exit coordinates are plotted in Fig.3. The nozzle and its chevron counterparts were rapid-prototyped using high-definition stereolithography with a tolerance (layer thickness) of 0.178 mm. The HWB planform was manufactured from a 3.2-mm thick aluminum sheet preserving the essential dimensions for shielding. It was mounted on a longitudinal traverse that permits the axial displacement of the shield relative to the nozzle.

For the experiments of this report, the following parameters were varied:

- *Nozzle axial location*. The fan exit plane was situated at normalized distances $X/D_s$=2.3, 3.3, and 4.3 upstream of the shield trailing edge, with $X$ denoting the distance from the fan exit plane to the trailing edge on the vertical plane through the nozzle centerline.
- *Design of vertical fins*. The nominal and alternate designs depicted in Fig. 2 were tested. The idea of the alternate design is to increase the length of the shield (chord length of the fin) while maintaining its aerodynamic effectiveness. In addition, tests were done with the fins removed. The dihedral angle of all the verticals was 79°.
- *Nozzle devices*. Chevrons and a wedge-shaped fan flow deflector were integrated into the baseline nozzle to modify the noise source. Figure 4 displays the nozzle modifications. The chevrons, designed by Boeing, featured ten serrations with a 20° insertion angle along the lips of the fan and core nozzles, thus they are of the aggressive type. The wedge-shaped fan flow deflector had a half angle of 18°, height (above core nacelle) of 5 mm, and length of 13 mm. The wedge apex was placed 3.0 mm downstream of the fan exit plane. The wedge was fabricated from a fine interwoven metal mesh with a mesh size of 0.223 mm and porosity of 49.6%. The basic function of the wedge is to reshape the mean flow such that velocity gradients are reduced in the downward and sideline directions, hence reducing turbulent kinetic energy and sound generation in those directions. A detailed investigation of porous wedge/flap fan flow deflectors can be found in Ref. 9. In addition, a combination of chevrons and wedge was also tested.

Figure 5 shows pictures of some of the shield/nozzle configurations tested in this program. Table 2 presents all the configurations tested along with the reductions in Effective Perceived Noise Level (EPNL).

### B. Aeroacoustic Testing

The nozzles were attached to a dual-stream apparatus that delivers room-temperature mixtures of helium and air to the primary (core) and secondary (bypass) nozzles. Helium-air mixtures have been shown to accurately duplicate the acoustics of hot jets[10]. The exit flow conditions, listed in Table 1, matched the typical exit conditions of a turbofan engine with bypass ratio 10 at takeoff power. The Reynolds number of the jet, based on fan diameter, was $0.68 \times 10^6$.

Noise measurements were performed in the aeroacoustic facility shown in Fig.6. The microphone array consists of twenty four 3.2-mm condenser microphones (Bruel & Kjaer, Model 4138). For acoustic surveys, the microphones were arranged twelve on a downward arm (azimuth angle $\phi$=0°) and twelve on a sideline arm ($\phi$=60°). Fig. 6a depicts the configuration of the downward arm; the sideline arm is practically identical. On each arm, the measurement polar angle $\theta$ ranged approximately from 20 to 120 deg relative to the downstream jet axis. This arrangement enabled simultaneous measurement of the downward and sideline noise at all the polar angles of interest. The sideline surveys were conducted in the half-space for which the nozzle is proximal to the vertical fin. For noise source mapping, the 24 microphones were aggregated on a dense linear array as shown in Fig. 6b. The polar aperture was 27.5 deg, with the first microphone at $\theta$=47.5° and the last microphone at $\theta$=73.0°.

The microphones were connected, in groups of four, to six conditioning amplifiers (Bruel & Kjaer, Model 2690-A-0S4). The 24 outputs of the amplifiers were sampled simultaneously, at 250 kHz per channel, by three eight-channel multi-function data acquisition boards (National Instruments PCI-6143). National Instruments LabView software was used to acquire the signals. The temperature and humidity inside the anechoic chamber were recorded to enable computation of the atmospheric absorption.

The narrowband sound pressure level spectra were corrected for actuator response, free-field correction, and atmospheric absorption. Overall sound pressure levels (OASPL) were obtained by integrating the corrected spectra. The conditions used for the Perceived Noise Level (PNL) and Effective Perceived Noise Level (EPNL) calculations are shown in Fig.7 and reflect the typical takeoff profile for the HWB. The microphone measurements in the downward ($\phi$=0$^o$) and sideline ($\phi$=60$^o$) directions were used respectively to assess the downward and sideline EPNL. Details of the EPNL calculation procedure can be found in Ref. 9. Noise source maps of the jets were generated from the deconvolution of the delay-and-sum beamformed output of the microphone array (Fig. 6b), using the method of Ref. 11.

## III. Results

### A. Detailed Acoustics

In this subsection we present acoustic summaries comprising the following quantities: narrowband lossless spectra, scaled to full-scale frequency (scale factor of 90), at selected polar angles; directivity of OASPL; PNL versus time; PNL versus observer polar angle; and estimate of EPNL. These quantities are compared against their respective baseline values (red curves). We compare the acoustics of shielded jets with the acoustics of the plain isolated nozzle for the downward ($\phi$=0$^o$) and sideline ($\phi$=60$^o$) directions. This gives an assessment of the overall benefit of shielding. The nozzle position was at its nominal location of $X/D_s$=2.3 and the nominal verticals were used.

Shielding of the plain nozzle, Fig. 8, produces benefits only at large polar angles and high frequency. The EPNL benefit is modest at 1.0 dB downward and 0.9 dB sideline. With application of the wedge (W18), Fig.9, we note a substantial improvement, with EPNL reductions of 4.6 dB downward and 3.4 dB sideline. The aggressive chevrons (AC), Fig. 10, offer slightly better reduction over the wedge, of 5.0 dB downward and 4.1 dB sideline. The crossover at small polar angles is caused primarily by the excess noise from the chevrons at high-frequency. The combination of chevrons and wedge (AC+W18), Fig. 11, offers the best overall EPNL reductions of 5.7 dB downward and 3.9 sideline. The EPNL reductions with nozzle devices are about 1 dB better (in each azimuthal direction) than for the N2A planform, indicating the acoustic superiority of the N2AEXTE design.

Now we assess the role of the vertical fins in jet noise shielding. Figure 12 presents acoustic summaries with the verticals removed. The nozzle used the AC+W18 devices. In comparing with Fig. 11 (installed verticals, everything else same), we note slightly better EPNL reduction in the downward direction (6.0 dB) but severely degraded EPNL reduction in the sideline direction (only 1.4 dB). It is evident that the vertical fins are essential for sideline noise reduction of the N2AEXTE.

### B. Insertion Loss

The deconvolution procedure of Ref. 11 yields high-resolution noise source distributions $q(Sr, x/D_s)$. They are presented here in the normalized form $q(Sr, x/D_s)/q_{max}(Sr)$ that helps identify the location of peak noise versus frequency. Figure 13 presents noise source distributions plain, chevron, and wedge nozzles. For the plain nozzle, the peak noise source location is practically constant at $x/D_s$=4.0 up to $Sr$=6, then it drops abruptly to $x/D_s$= −1 (it should be kept in mind that here $x$ is defined relative to plug tip, so $x/D_s$= −1 denotes the fan exit plane). This sudden transition has been observed in the past in phased array measurements of full-scale high-bypass turbofan engines[12]. Application of the aggressive chevrons makes a notable change in the noise source location, moving the transition Strouhal number to $Sr$≈1.2. In contrast to the abrupt transition in the peak noise source location with the chevrons, the wedge induces a more gradual trend of reduction in noise source length. These trends have direct consequences on the insertion loss, discussed next.

Insertion loss data are presented as contour maps of the difference in sound pressure level between a given nozzle in isolation and the same nozzle with shield, plotted against polar angle $\theta$ and Strouhal number $Sr$. Black lines represent insertion loss of 3 dB. In Fig. 14 we examine the insertion loss in the downward direction for the nominal shield configuration for different nozzle designs. For the plain nozzle, the insertion loss map shows very small values except at high polar angles. The larger insertion loss at high frequency is associated with the noise source moving upstream closer to the fan exit plane. Application of the aggressive chevrons makes a notable change in the noise source location, moving the transition Strouhal number to $Sr$ ≈ 1.2. The insertion loss map shows very significant levels starting at $Sr$≈1.2. The insertion loss for the wedge is more modest than for the

chevrons. However, the wedge being quieter in isolation, the EPNL shielding benefits of the two devices are similar.

In Fig. 15 we assess the impact of the vertical fin, and its design variations, on sideline insertion loss, using the chevron nozzle. With the fins removed, the sideline insertion loss is minimal, consistent with the small sideline EPNL reductions noted in Table 2. The nominal fin design provides significant insertion loss (> 3 dB) for $50^o < \theta < 100^o$ and $Sr > 2$. The alternate fin design broadens this range of polar angle and increases the overall level of insertion loss. Thus the increased chord length of the alternate fin design has a measurable impact on sideline shielding, although the improvement in EPNL is modest.

### C. EPNL Reduction Trends

To optimize the propulsion integration of the turbofan-powered HWB, the designer needs to know the relative benefits of nozzle devices versus axial placement of the engines, as well as the effects of the vertical fins on noise suppression. We attempt to provide this information in Figs. 16-18. In each figure, we plot the EPNL reduction (downward, sideline, and cumulative = downward+sideline) versus axial placement $X/D_s$ of the fan exit plane relative to the trailing edge. Figures 16, 17, and 18 consider the shield configurations without verticals, with nominal verticals, and with alternate verticals, respectively. Focusing in the downward direction (left columns of all the figures), we note that the benefit of forward placement of the engine is connected to the aggressiveness of the nozzle device. For the plain nozzle, moving the engine upstream by two fan diameters we gain only 1 dB reduction in EPNL. This benefit goes up to 3 dB for the AC+W18 nozzle. In general, however, we note that modifying the nozzle is a much more effective way to suppress noise than moving the engine upstream. As far as downward reductions are concerned, the presence and designs of the vertical fins have very small impact.

On the other hand, sideline reductions (middle column) are affected strongly by the presence of the verticals, and to a lesser extent by their designs. Without verticals (Fig.16), the maximum sideline EPNL reduction is 2.2 dB using the wedge nozzle. The axial nozzle placement has practically no effect on the sideline reduction without the verticals. With the nominal verticals (Fig.17), nozzle configurations including the chevrons show a maximum sideline reduction at $X/D_s$=3.3 (i.e., the nozzle is moved forward by one fan diameter). This suggests an optimal integration of the vertical and the chevron nozzle at that location. Alternatively, if the engine were to stay at its nominal location, the optimal location of the fin would be one fan diameter aft of its present location. This trend is particularly noticeable for the alternate vertical (Fig. 18), with the optimization yielding an additional 1 dB in sideline reduction, using either the chevron (AC) nozzle or the combination (AC+W18) nozzle. Examining the cumulative EPNL reductions in Figs. 16-18, we note diminishing returns for the engine moving forward past one fan diameter.

Looking at the general picture portrayed by Figs. 16-18, and Table 2, we see a very encouraging potential of reducing cumulative EPNL by up to 10 dB with the engines at nominal location and 13 dB with the engines moved forward. Nozzle devices (chevrons, wedge) and vertical fins are essential for achieving these reductions.

## IV. Concluding Remarks

The advanced N2AEXTE design of the Hybrid Wing-Body airplane offers very promising potential for jet noise shielding. Our subscale static experiments show cumulative EPNL reductions of up to 10 dB with the nozzle at its nominal position and up to 13 dB with the nozzle moved forward by one fan diameter. These reductions are 2-3 dB better than with the basic N2A design. Redistribution/compaction of the jet noise source and incorporation of inboard vertical fins are essential elements for achieving those reductions. Devices used to alter the jet noise source comprised aggressive chevrons, a porous wedge fan flow deflector, and their combination. Two shapes for the vertical fins were tested - a nominal design and an alternate design featuring longer chord and shorter height. The alternate fin design offered slight noise benefits.

This study and its predecessor[6] underscore the importance of nozzle devices to compact and redistribute the noise source. Even though the resulting noise reductions are substantial, they come at a performance cost which this study did not address. The thrust penalty of the porous wedge deflector is estimated at 0.5% and, with a deployable wedge (flaps), it would be suffered for only the takeoff phase of the flight[9]. The aerodynamic penalty of the aggressive chevrons is unknown at this time, but it is probably not small; this penalty would be sustained over the entire flight unless the chevrons are deployable as well, a rather complex undertaking.

The effect of forward flight comes up often when one assesses acoustic performance based on static tests. Forward flight has aerodynamic effects on the jet flow field and acoustic propagation effects on the diffraction pattern. For the plain jet, the aerodynamic effect elongates the jet noise source. However, when using aggressive

devices such as the chevrons and wedge of this study, the location of peak noise at moderate to high frequency (Fig. 13) is unlikely to be displaced significantly. With regards to changes in the diffraction pattern (for a fixed noise source), the low takeoff Mach number of around 0.2 is not expected to affect significantly the insertion loss. Indeed the canonical experiments of Von Glahn et al.[3] showed minimal impacts of forward flight on jet noise shielding, particularly when mixer devices were used. Nevertheless, the effect of forward flight on a complex airframe-propulsion system such as the HWB deserves further study.

**Acknowledgment**

This research was funded by Boeing Subcontract No. 208547 in support of NASA contract NNL07AA54C "Acoustic Prediction Methodology and Test Validation for an Efficient Low-Noise Hybrid Wing Body Subsonic Transport."

**References**

1. Liebeck, R.H., "Design of the Blended Wing Body Subsonic Transport," *Journal of Aircraft*, Vol. 41, No. 1, Jan.–Feb. 2004.
2. Von Glahn, U., Groesbeck, D., and Reshotko, M., "Geometry Considerations for Jet Noise Shielding with CTOL Engine-Over-The-Wing Concept," AIAA Paper 74-568, June 1974.
3. Von Glahn, U., Goodykoontz, J., and Wagner, J., "Nozzle Geometry and Forward Velocity Eeffects on Noise for CTOL Engine-Over-The-Wing Concept," NASA TM-X-71453, Oct. 1973
4. Von Glahn, U., Groesbeck, D., and Wagner, J., "Wing Shielding of High-Velocity Jet and Shock-Associated Noise with Cold and Hot Flow Jets," AIAA Paper 76-547, July 1976.
5. Papamoschou, D., and Mayoral, S., "Experiments on Shielding of Jet Noise by Airframe Surfaces," AIAA Paper 2009-3326, May 2009.
6. Mayoral, S., and Papamoschou, D., "Effects of Source Redistribution on Jet Noise Shielding," AIAA Paper 2010-0652, Jan. 2010.
7. Papamoschou, D., "Prediction of Jet Noise Shielding," AIAA Paper 2010-0653, Jan. 2010.
8. Czech, M.J., Thomas, R.H., and Elkoby, R., "Propulsion Airframe Aeroacoustic Integration Effects for a Hybrid Wing Body Aircraft Configuration," AIAA Paper 2010-3912, June 2010.
9. Papamoschou, D., "Pylon Based Jet Noise Suppressors," *AIAA Journal*, Vol. 47, No. 6, 2009, pp. 1408-1420.
10. Papamoschou, D., "Acoustic Simulation of Coaxial Hot Air Jets Using Cold Helium-Air Mixture Jets," *Journal of Propulsion and Power*, Vol. 23, No.2, 2007, pp. 375-381.
11. Papamoschou, D., "Imaging of Distributed Directional Noise Sources," AIAA Paper 2008-2885, May 2008.
12. Brusniak, L., Underbrink, J.R., and Nesbitt, E., "Phased Array Measurements of Full-Scale Exhaust Noise," AIAA Paper 2007-3612, May 2007.

**Table 1 Cycle conditions for the BPR10 jet**

| Quantity | Core | Fan |
|---|---|---|
| NPR | 1.376 | 1.550 |
| NTR* | 2.950 | 1.139 |
| $T_0$ ($^o$K)* | 864 | 334 |
| $T$ ($^o$K)* | 781 | 291 |
| $M$ | 0.691 | 0.817 |
| $U$ (m/s) | 387 | 279 |

*Equivalent conditions using helium-air mixture jets

**Table 2 Configurations tested and EPNL reductions relative to isolated plain nozzle**

**No Verticals**

| | PLAIN | | | W18 | | | AC | | | AC+W18 | | |
|---|---|---|---|---|---|---|---|---|---|---|---|---|
| $X/D_s$ | $\Delta EPNL_D$ | $\Delta EPNL_S$ | $\Delta EPNL_C$ | $\Delta EPNL_D$ | $\Delta EPNL_S$ | $\Delta EPNL_C$ | $\Delta EPNL_D$ | $\Delta EPNL_S$ | $\Delta EPNL_C$ | $\Delta EPNL_D$ | $\Delta EPNL_S$ | $\Delta EPNL_C$ |
| 2.3 | 1.0 | 0.3 | 1.3 | 4.6 | 2.2 | 6.7 | 5.1 | 1.5 | 6.6 | 6.0 | 1.4 | 7.4 |
| 3.3 | - | - | - | 5.5 | 2.3 | 7.9 | 6.5 | 1.9 | 8.3 | 7.7 | 1.6 | 9.3 |
| 4.3 | 1.0 | 0.9 | 1.9 | 6.5 | 2.7 | 9.2 | 7.3 | 2.3 | 9.6 | 8.9 | 2.2 | 11.0 |

**Nominal Verticals**

| | PLAIN | | | W18 | | | AC | | | AC+W18 | | |
|---|---|---|---|---|---|---|---|---|---|---|---|---|
| $X/D_s$ | $\Delta EPNL_D$ | $\Delta EPNL_S$ | $\Delta EPNL_C$ | $\Delta EPNL_D$ | $\Delta EPNL_S$ | $\Delta EPNL_C$ | $\Delta EPNL_D$ | $\Delta EPNL_S$ | $\Delta EPNL_C$ | $\Delta EPNL_D$ | $\Delta EPNL_S$ | $\Delta EPNL_C$ |
| 2.3 | 1.0 | 0.9 | 1.9 | 4.5 | 3.4 | 8.0 | 4.9 | 4.2 | 9.1 | 5.7 | 4.0 | 9.7 |
| 3.3 | - | - | - | 5.3 | 3.6 | 8.9 | 6.1 | 4.4 | 10.5 | 7.5 | 4.3 | 11.8 |
| 4.3 | 2.2 | 1.4 | 3.6 | 6.4 | 4.0 | 10.4 | 7.1 | 3.9 | 11.0 | 9.1 | 3.9 | 13.0 |

**Alternate Verticals**

| | PLAIN | | | W18 | | | AC | | | AC+W18 | | |
|---|---|---|---|---|---|---|---|---|---|---|---|---|
| $X/D_s$ | $\Delta EPNL_D$ | $\Delta EPNL_S$ | $\Delta EPNL_C$ | $\Delta EPNL_D$ | $\Delta EPNL_S$ | $\Delta EPNL_C$ | $\Delta EPNL_D$ | $\Delta EPNL_S$ | $\Delta EPNL_C$ | $\Delta EPNL_D$ | $\Delta EPNL_S$ | $\Delta EPNL_C$ |
| 2.3 | 1.1 | 0.9 | 2.0 | 4.7 | 3.3 | 7.9 | 5.0 | 3.9 | 8.9 | 5.9 | 3.9 | 9.8 |
| 3.3 | - | - | - | 5.5 | 3.8 | 9.3 | 6.3 | 5.1 | 11.4 | 7.6 | 5.3 | 12.9 |
| 4.3 | 2.3 | 1.4 | 3.7 | 6.5 | 4.1 | 10.6 | 7.1 | 4.5 | 11.6 | 9.0 | 4.8 | 13.8 |

PLAIN = Plain BPR10 nozzle
W18 = BPR10 nozzle with 18-deg porous wedge
AC = BPR10 nozzle with aggressive chevrons
AC+W18 = BPR10 nozzle with aggressive chevrons and 18-deg wedge.
$\Delta EPNL_D$ = Reduction in downward EPNL
$\Delta EPNL_S$ = Reduction in sideline EPNL
$\Delta EPNL_C$ = Reduction in cumulative (downward+sideline) EPNL

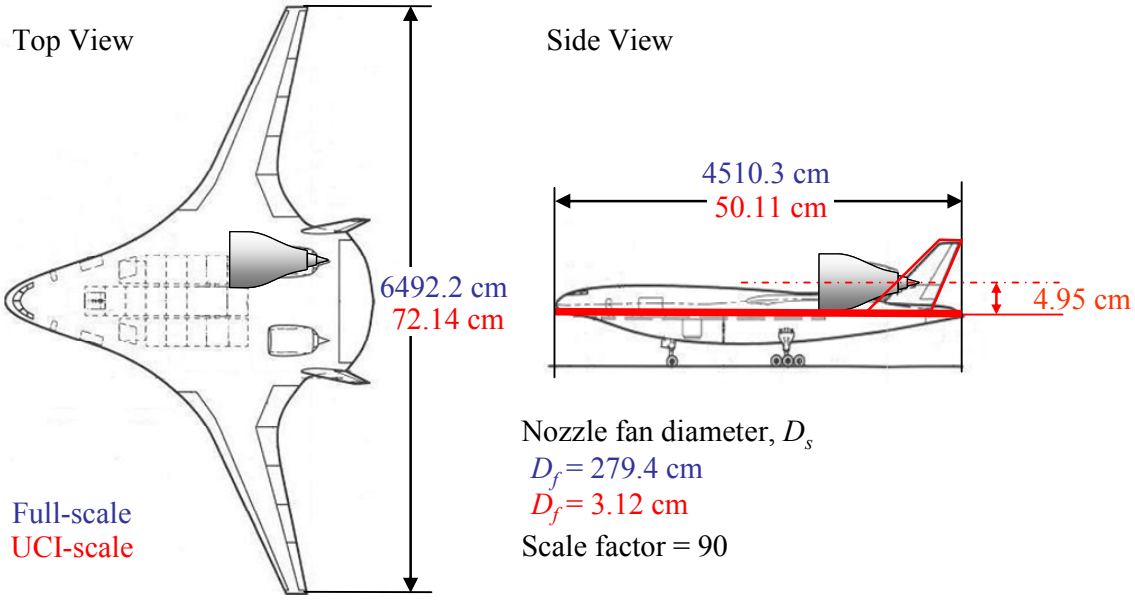


**Fig. 1 Scaling of HWB planform to UCI dimensions and retention of critical dimensions for shielding (red lines).**

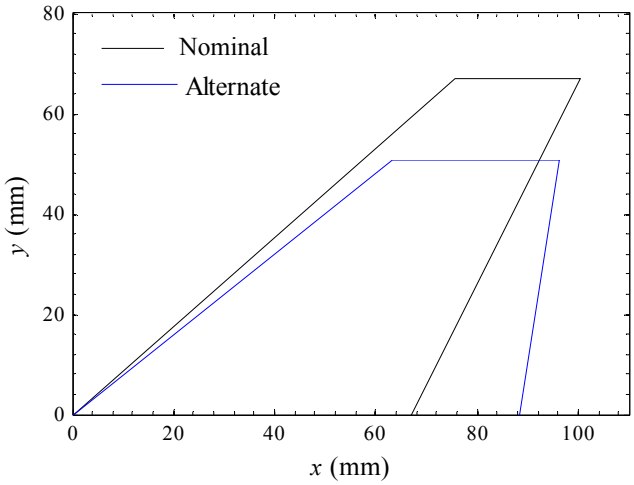


**Fig. 2 Designs of nominal and alternate vertical fins.**

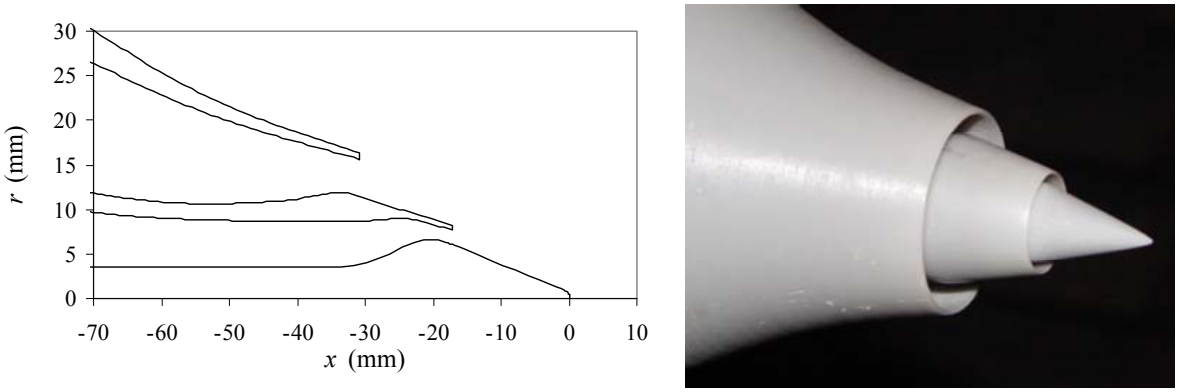


**Fig. 3 Coordinates and picture of BPR10 nozzle.**

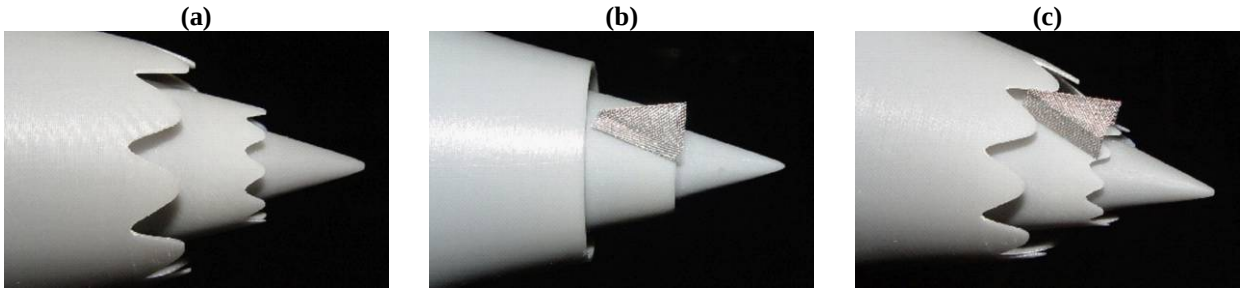


**Fig. 4 Nozzle modifications. (a) Aggressive chevrons (AC); (b) porous wedge with 18-deg half angle (W18); and (c) combination (AC+W18).**

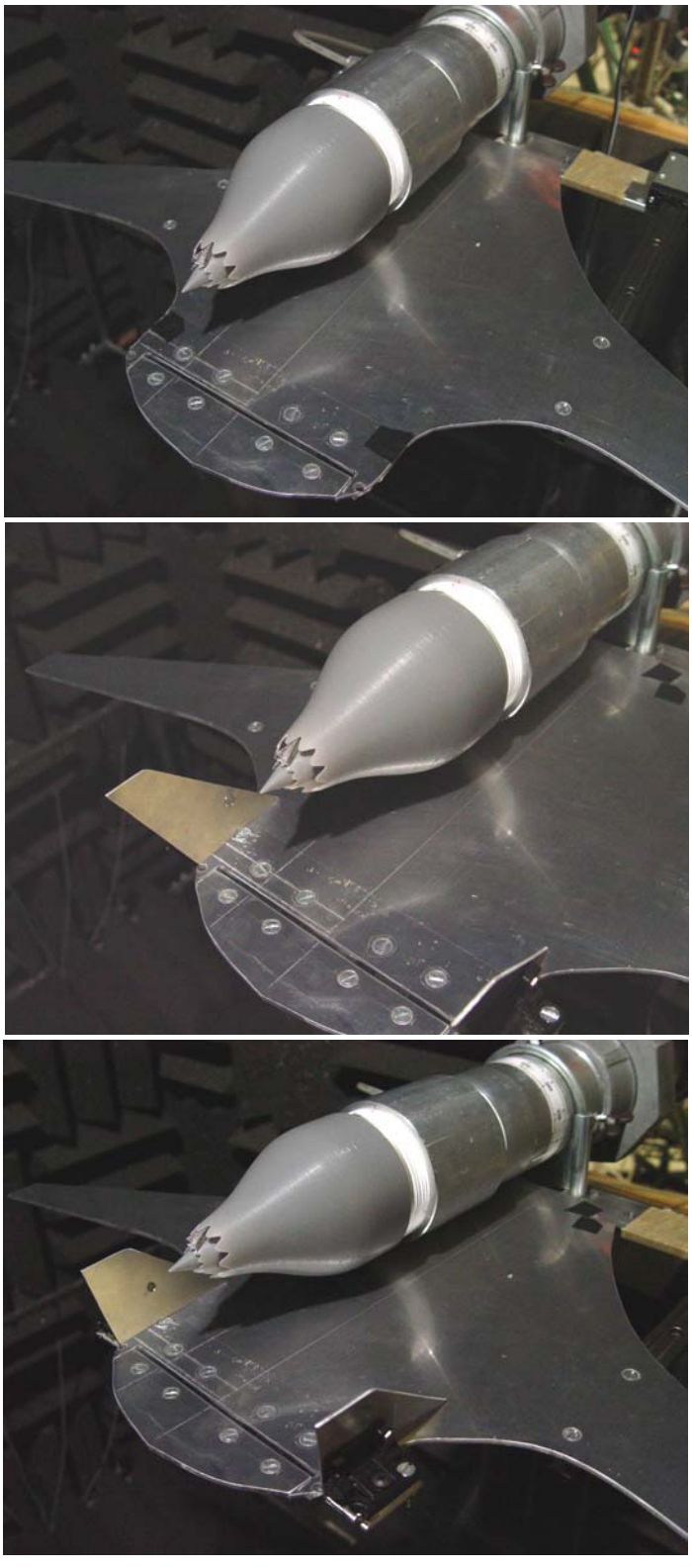


**Fig.5 Photos of experimental configurations with combination (AC+W18) nozzle. (a) No verticals; (b) nominal verticals; (c) alternate verticals.**

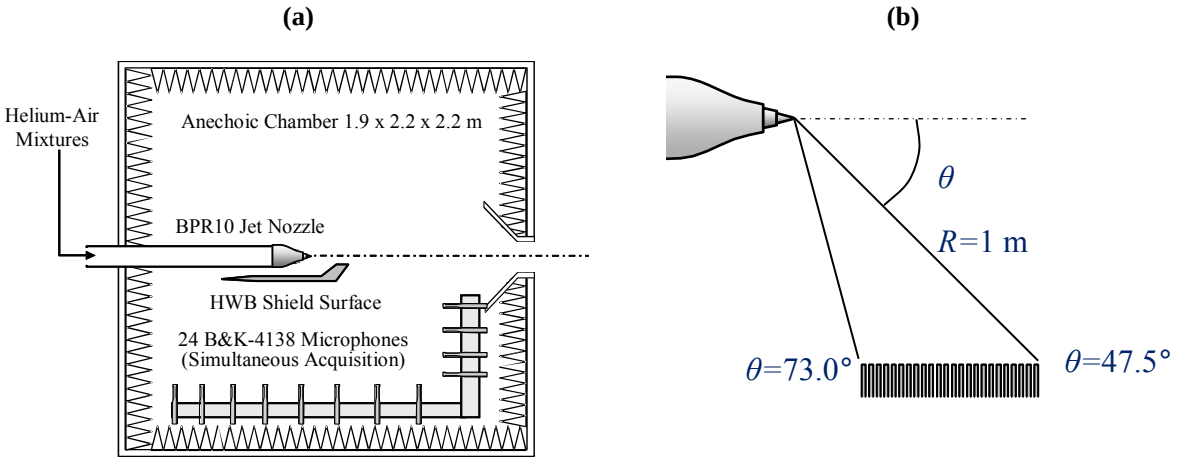


**Fig. 6 Aeroacoustic measurement. (a) Setup for acoustic surveys; (b) setup for noise source imaging.**

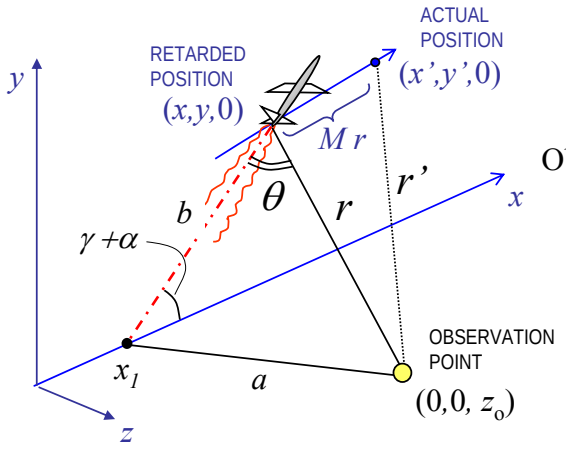


Aircraft flying with Mach number $M$, angle of attack $\alpha$, and climb angle $\gamma$

Observation distance and polar emission angle

$$r' = \sqrt{x'^2 + y'^2 + z_0^2}$$

$$r = \sqrt{x^2 + y^2 + z_0^2}$$

$$\tan(\theta/2) = \sqrt{\frac{(p-b)(p-r)}{p(p-a)}}$$

where

$$x_1 = x - y/\tan(\gamma+\alpha)$$

$$a = \sqrt{x_1^2 + z_0^2}$$

$$b = y/\sin(\gamma+\alpha)$$

$$p = \frac{1}{2}(a+b+r)$$

| CONDITIONS FOR EVALUATON OF PNL | | |
|---|---|---|
| | SIDELINE | CUTBACK |
| Lateral distance, $z_0$= | 1476 ft | 0 ft |
| Altitude at $x$=0 | 1500 ft | 2171 ft |
| Angle of attack, $\alpha$= | 13.35º | 13.93º |
| Climb angle, $\gamma$= | 9.46º | 2.29º |
| Flight Mach, $M$= | 0.220 | 0.224 |

**Fig. 7 Geometric relations and conditions for assessment of perceived noise level.**

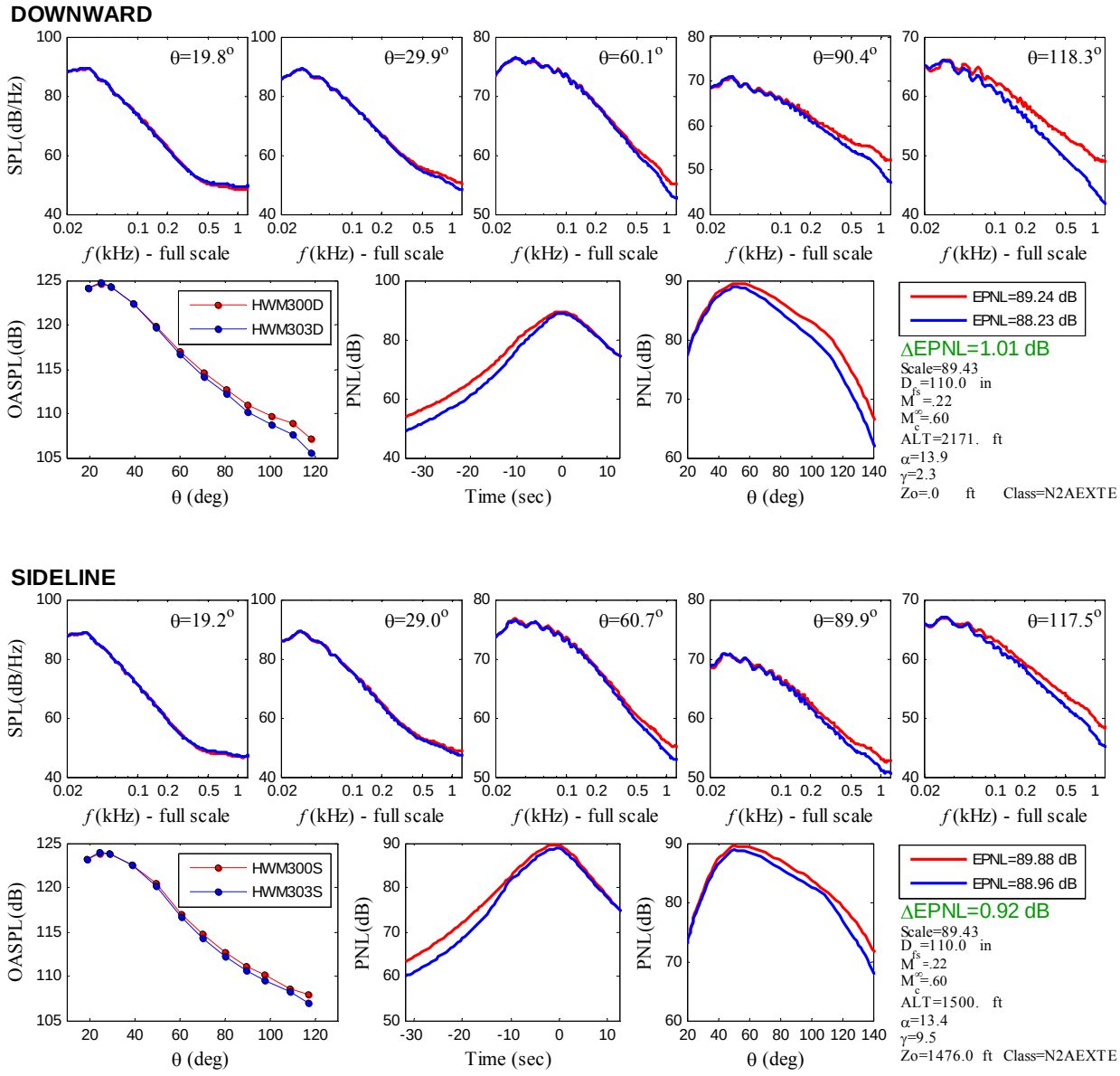


**Fig. 8 Acoustics of shielded plain nozzle (blue) compared to isolated plain nozzle (red). Nominal verticals and nominal nozzle location.**

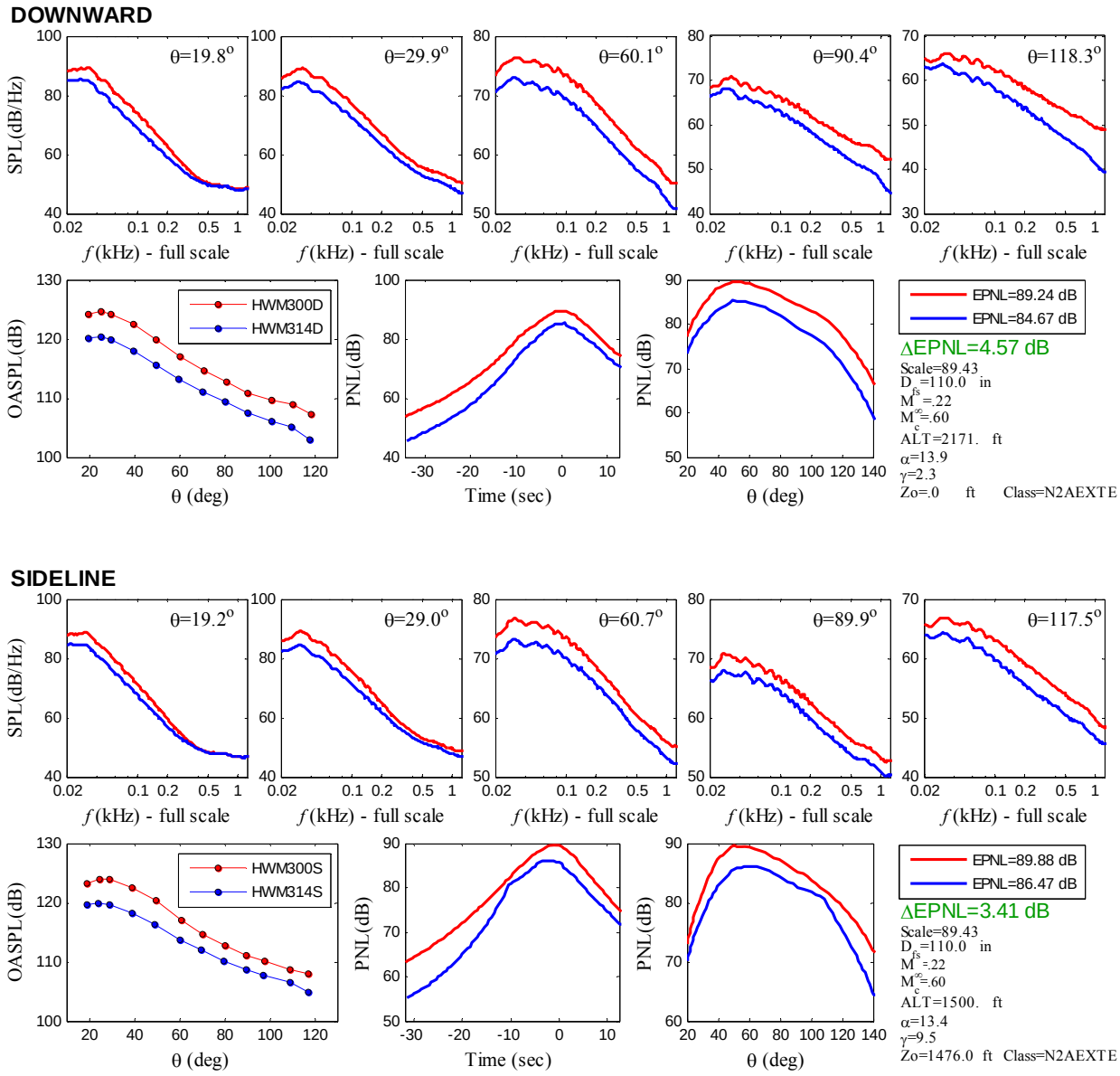


**Fig. 9 Acoustics of shielded wedge nozzle (blue) compared to isolated plain nozzle (red). Nominal verticals and nominal nozzle location.**

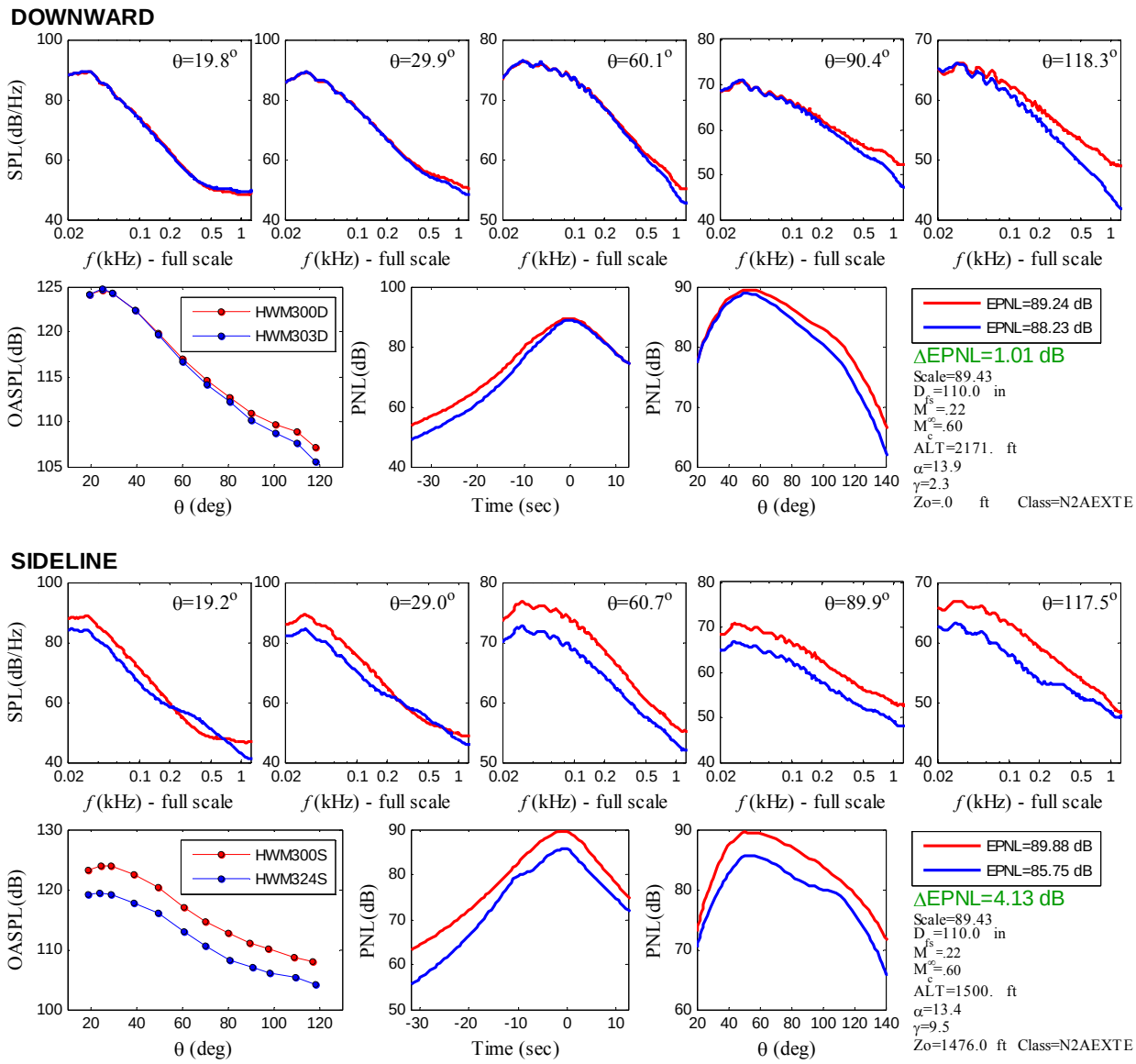


**Fig. 10 Acoustics of shielded chevron nozzle (blue) compared to isolated plain nozzle (red). Nominal verticals and nominal nozzle location.**

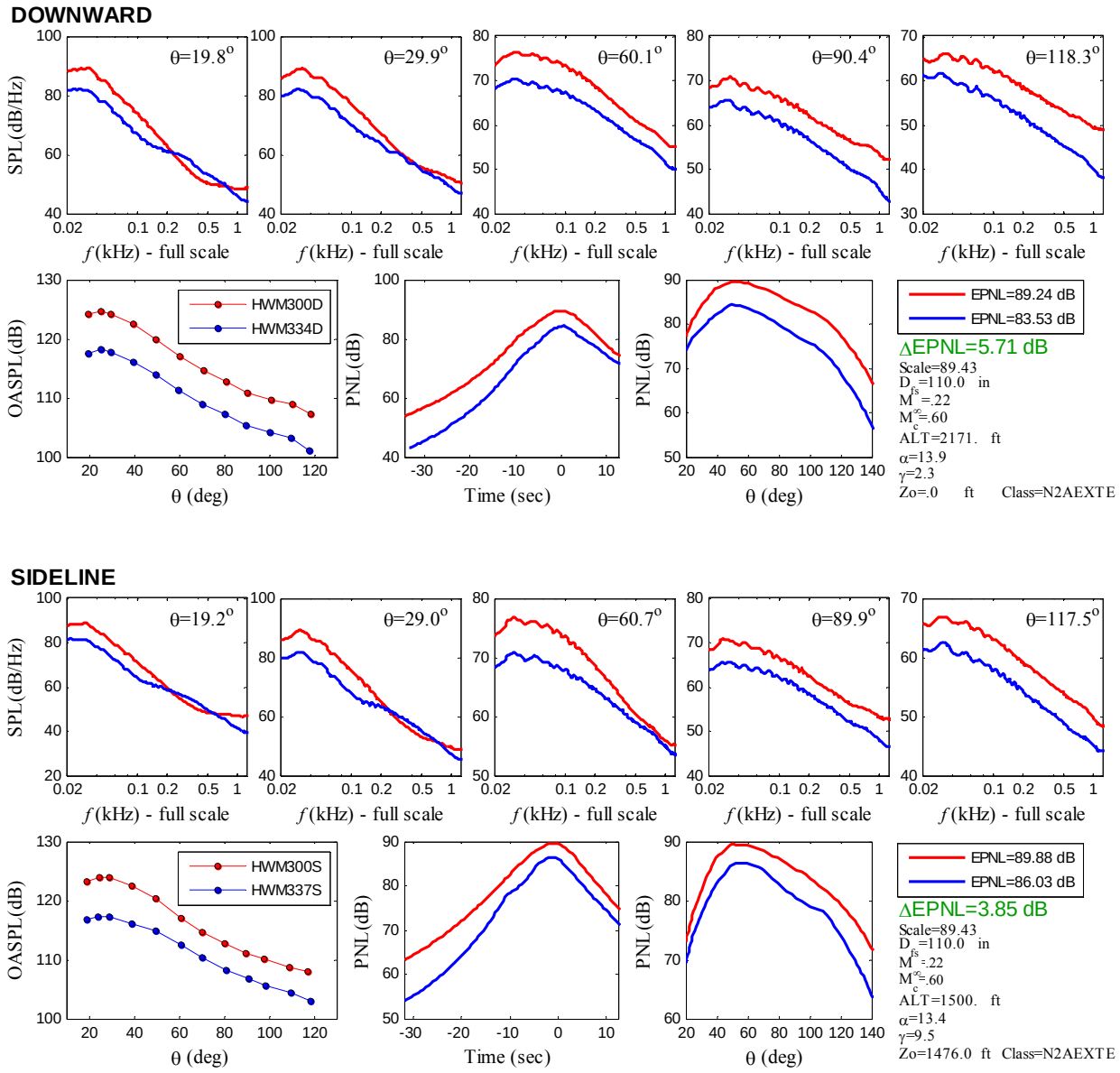


**Fig. 11 Acoustics of shielded combination nozzle (blue) compared to isolated plain nozzle (red). Nominal verticals and nominal nozzle location.**

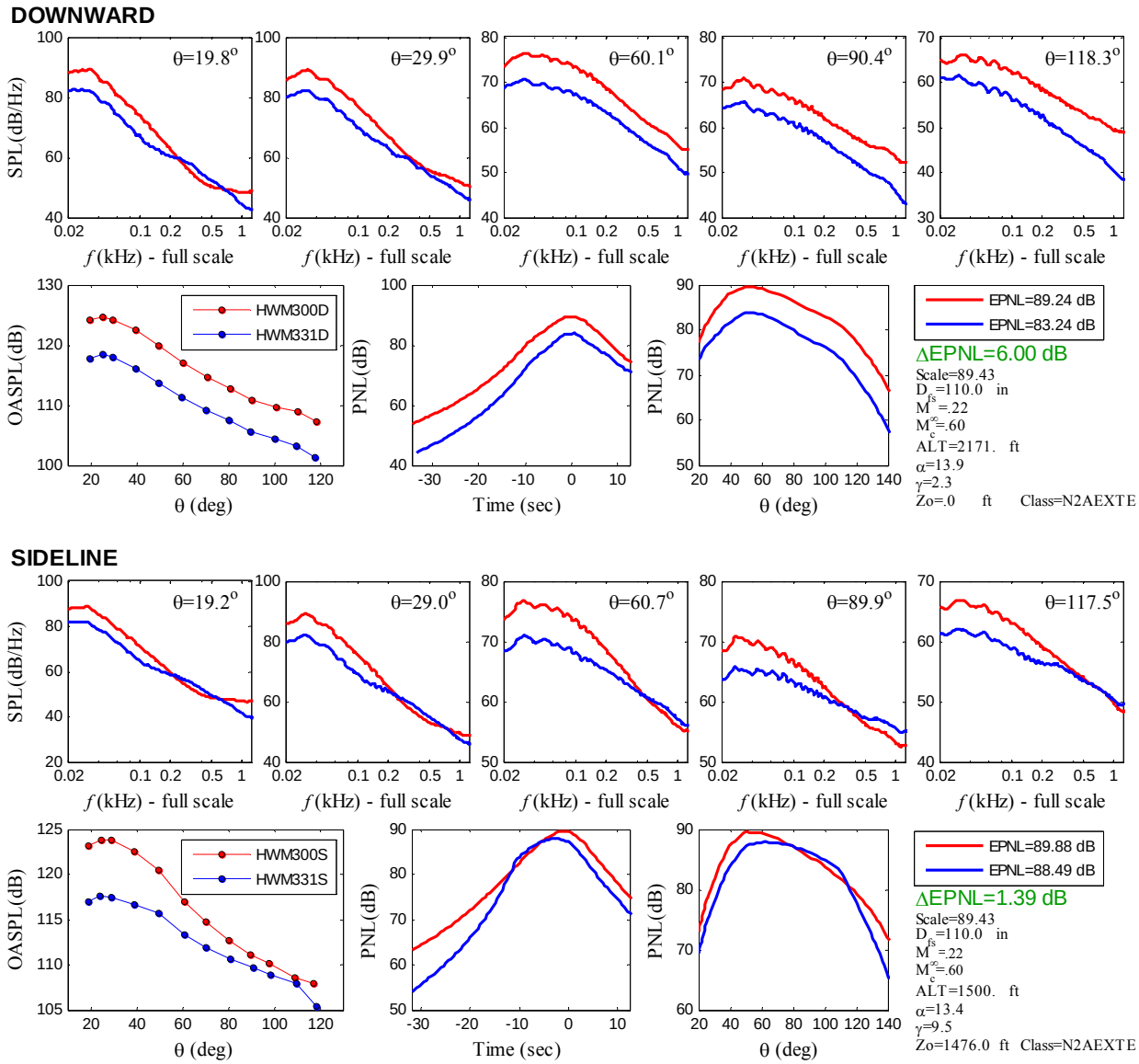


**Fig. 12 Acoustics of shielded combination nozzle (blue) compared to isolated plain nozzle (red). Nominal nozzle location, no verticals.**

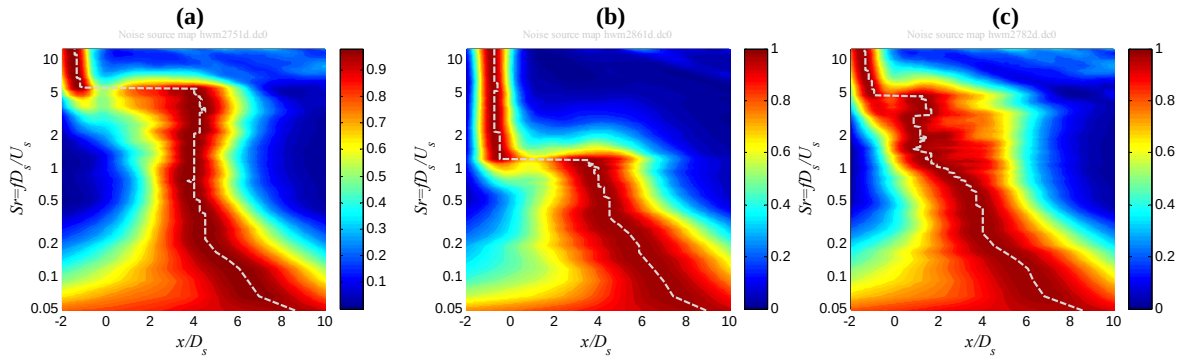


**Fig. 13 Noise source distributions for isolated BPR10 jets, with dashed white lines indicating location of peak noise. (a) Plain nozzle; (b) aggressive chevrons; (c) porous wedge.**

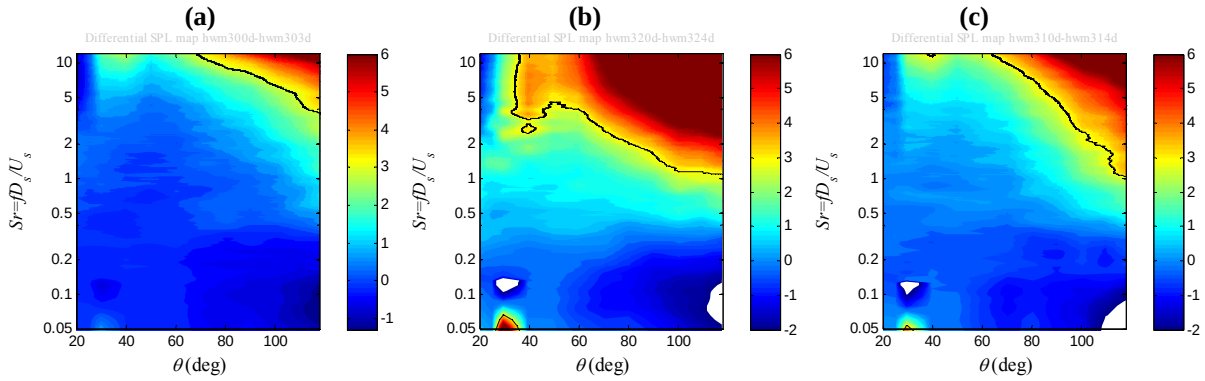


**Fig. 14 Insertion loss (dB) for noise in the downward direction, using nominal verticals with nozzle at nominal location $X/D_s$=2.3. (a) Plain nozzle; (b) aggressive chevrons; (c) porous wedge. Black line indicates insertion loss of 3 dB.**

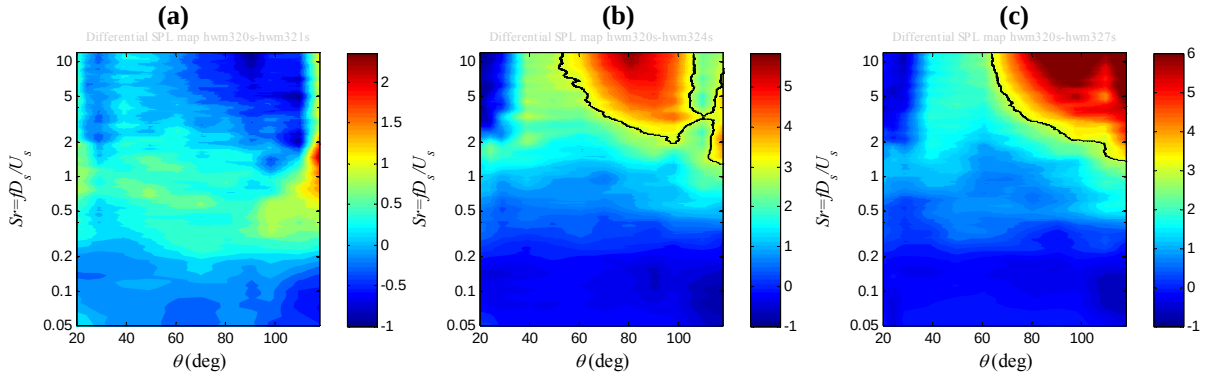


**Fig. 15 Insertion loss (dB) for noise in the sideline direction, using aggressive chevron nozzle at nominal location $X/D_s$=2.3. (a) No verticals; (b) nominal verticals; (c) alternate verticals. Black line indicates insertion loss of 3 dB.**

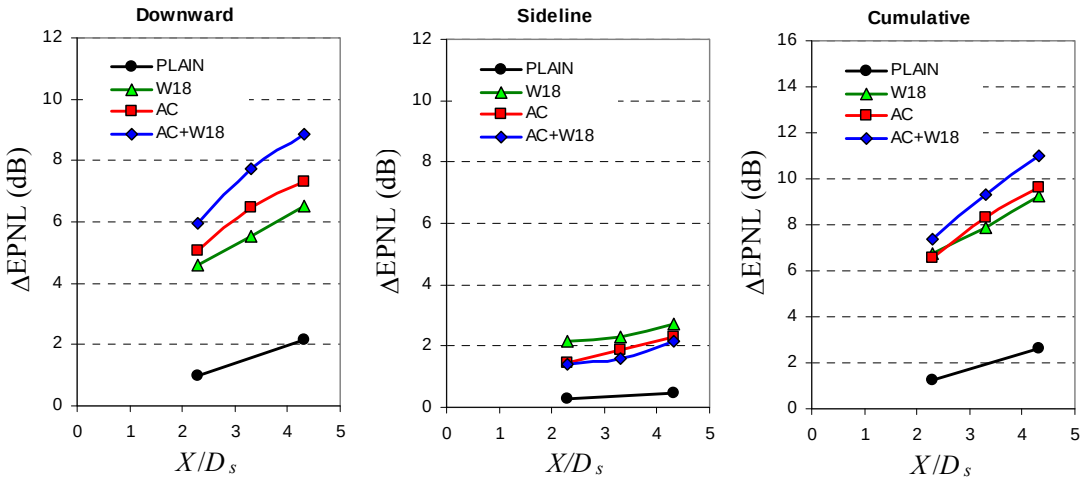


**Fig. 16 EPNL reductions versus axial position of fan exit plane relative to trailing edge. Shield without verticals.**

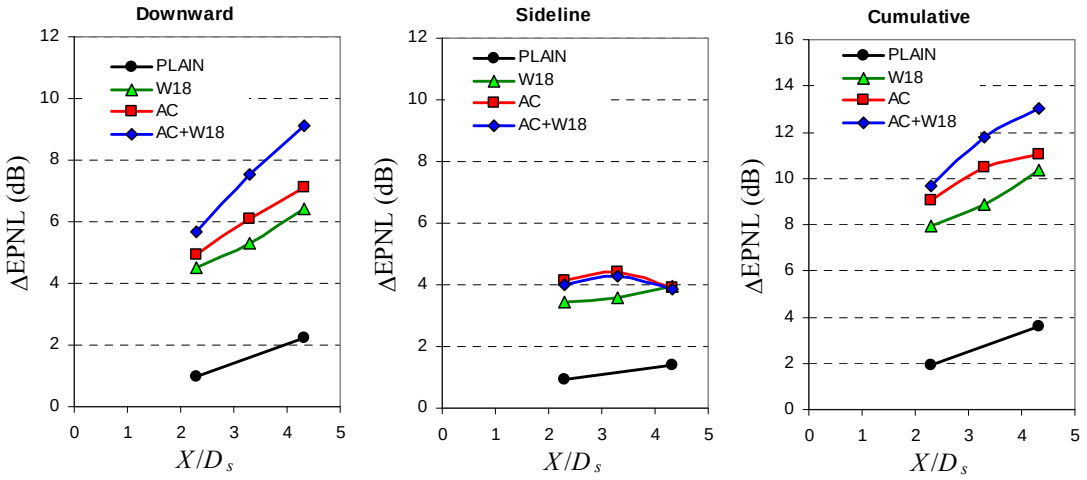


**Fig. 17 EPNL reductions versus axial position of fan exit plane relative to trailing edge. Shield with nominal verticals.**

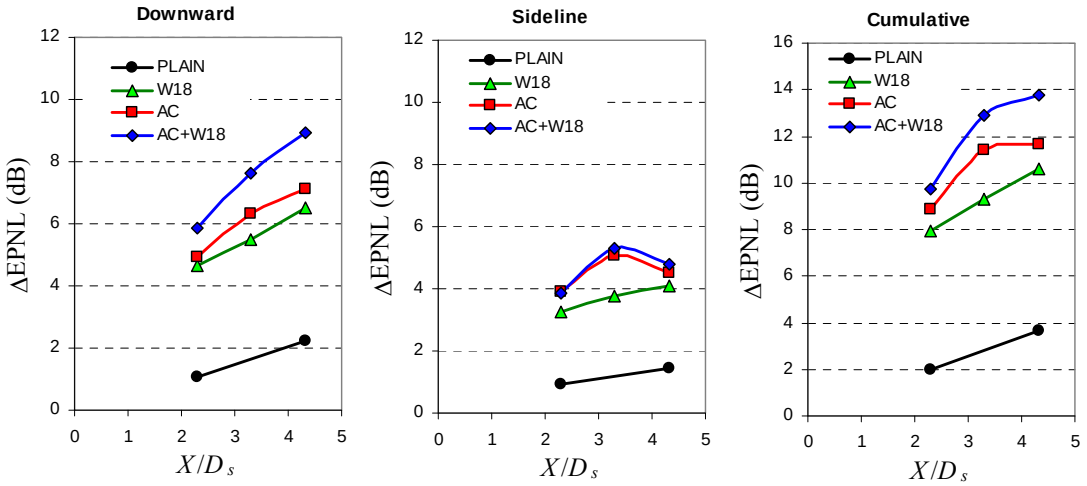


**Fig. 18 EPNL reductions versus axial position of fan exit plane relative to trailing edge. Shield with alternate verticals.**